ALiSA: a Visible-Light Positioning System using the Ambient Light Sensor Assembly in a Smartphone

Takuto Sato, Shota Shimada, Hiroaki Murakami, Hiroki Watanabe, Hiromichi Hashizume, *Member, IEEE*, and Masanori Sugimoto, *Member, IEEE*

***Abstract*— In this paper , we describe a visible-light positioning system that uses the ambient-light sensor assembly in a smartphone as a receiver for illumination signals from LED-based room lighting. After correcting for missing or inconsistently sampled data captured by the receiver, we can identify the source LEDs contributing to the received signal via Fourier analysis of its frequency distribution. Localization of the smartphone is then achieved by trilateration of the distances to the various LEDs, which are calculated from the received signal strength for each LED. Experiments using multiple LEDs were conducted to evaluate the signal reception and positioning performance of the system. We found that multiple LEDs modulated at frequencies of over 70 Hz could be correctly identified from the received signal pattern. The 90th-percentile 2D positioning errors using low frequency signals (3.951-7.902 Hz) were less than 0.21 meter for a room illuminated by four LEDs arranged in a 1-m square on the ceiling at 2.22 meters height, where the smartphone was placed parallel on the floor from 1.4 meters height. Those using high frequency signals (111.619-114.582 Hz) in the same room setting showed 50th-percentile 2D position errors of less than 0.44 meter. The position calculation was offline and not implemented on real time. Potential applications and limitations of the proposed method are discussed.**

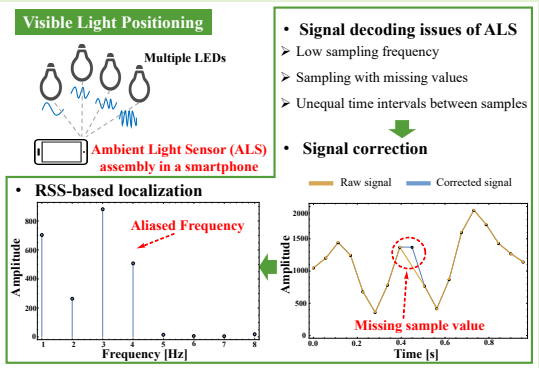

***Index Terms*— Indoor localization, visible light positioning (VLP), ambient light sensor (ALS), Received Signal Strength (RSS), smartphone .**

I. Introduction

By 2027, the global market for indoor positioning services is predicted to reach 56.6 billion dollars [1]. Indoor positioning services are deployed in a variety of applications, such as navigation, healthcare, advertising, and manufacturing. Due to the limitations of the Global Navigation Satellite System in indoor environments, various technologies leveraging signals such as radio waves, infrared, sound, and visible light have been proposed [2]. Of these, visible light positioning (VLP) based on visible light communication [3] [4] is attracting attention because of the widespread use and low price of devices based on light-emitting diodes (LEDs). Compared with other technologies such as radio waves, the advantages of VLP include sub-meter-level positioning accuracy, low-cost deployment and high security. International standardization related to VLP technologies [5] is being pursued actively, with the aim of encouraging their widespread adoption.

In a VLP system, a receiver identifies the transmitted signals from a number of LEDs, from which it calculates its own relative position. LED-based illumination is usually modulated at a frequency above 70 Hz (denoted F_{70}), which prevents the perception of optical flicker by human viewers. This is necessary because LED-based illumination is widely used in inhabited buildings [6]. The receiver in a VLP system is typically a complementary metal-oxide-semiconductor (CMOS) image sensor embedded in a camera or a high-speed photodiode (PD). If they are to be widely adopted, VLP systems should utilize commercial off-the-shelf (COTS) mobile devices as the receiver. However, for such COTS devices, CMOS cameras involve high power consumption and PDs require extra hardware or modification to the software running on the device. Therefore, practical VLP technologies for COTS devices such as smartphones have yet to be developed [7].

In this paper, we propose ALiSA, a VLP system based on received signal strength (RSS). ALiSA utilizes the ambient light sensor (ALS) assembly in a smartphone. ALS is widely used in smartphones for the purpose of adjusting screen brightness automatically, and consumes much less power than the receivers used in other devices such as cameras and high-

T. Sato, S. Shimada, H. Murakami, H. Watanabe and M. Sugimoto are with Graduate School of Information Science and Technology, Hokkaido University, Sapporo 060-0814, Japan (email: tsato@ist.hokudai.ac.jp; shimadas@eis.hokudai.ac.jp; hmurakami@ist.hokudai.ac.jp; hiroki.watanabe@ist.hokudai.ac.jp; sugi@ist.hokudai.ac.jp).

H. Hashizume is with National Institute of Informatics, Tokyo 101-8430, Japan (e-mail: has@nii.ac.jp).

speed PDs. However, the ALS assembly in a smartphone is seldom used as a VLP receiver because its sampling frequency is far lower than F_{70} and its sampling is unstable because of the constraints of the smartphone operating system (OS). In our proposal, the ALS captures the combined light signal from the LED devices on the ceiling of a room, where each LED is modulated at a specific frequency. From a discrete Fourier transform (DFT) analysis of the received signal, it can identify the individual LEDs by using the modulating frequency as the location identity (ID). The distance between each LED and the smartphone is calculated using the RSS value of each LED signal, from which the smartphone position can be estimated by the principle of trilateration. In this paper, we address two challenges related to signal decoding in our proposed system. First, sampling using the ALS assembly in a smartphone can miss sample values or involve unequal time intervals between samples (called "nonuniform sampling"). Unfortunately, these issues cannot be resolved or even alleviated through existing user application software. Instead, we investigate the sampling operation of different ALS assemblies in various smartphone models and evaluate methods for avoiding missing values and nonuniform sampling. Second, the sampling frequency of these ALS assemblies is very low, which prevents the DFT process from determining the correct transmitted signal frequencies. This is because of frequency aliasing, whereby a high-frequency signal is "aliased" to a low frequency band, causing the LED's ID to be confused with that of other LEDs. Thus, we estimate the correct frequency of the transmitted signal from its aliased frequency.

In our experiments, we first tested the effectiveness of two proposed methods for filling any missing sample values and a method for correcting for nonuniform sampling. We then measured the signal-to-noise ratio (SNR) of received signals to evaluate the signal reception performance of the ALS assembly in a smartphone. The results showed that the ALS could receive a light signal modulated at F_{70} and that missing values reduced the SNR of the received signal. We then tested ALiSA in several real environments, with various placement arrangements for the LEDs, to investigate its localization performance. In experiments conducted in a room where four LEDs were arranged in a 1-m square on the ceiling at 2.22 meters height and the smartphone was placed parallel on the floor from 1.4 meters height, the results obtained using low frequency signals (3.951-7.902 Hz) gave 90th-percentile 2D position errors of less than 0.21 m. Those using high frequency signals (111.619-114.582 Hz) in the same room setting showed 50th-percentile 2D position errors of less than 0.44 meter. The position calculation was offline and not implemented on real time.

From these experimental results, we discuss the potential applications and limitations of the proposed VLP method using an ALS assembly in a smartphone (see Section V).

Our contributions can be summarized as follows.

- As far as we know, this is the first proposal that uses the ALS assembly in a smartphone as a VLP receiver and evaluates its effectiveness and limitations.
- We propose two methods for addressing the missing-sample issue and a method for correcting for nonuniform sampling by the VLP receiver.
- We implemented ALiSA as a VLP system using the ALS assembly in a smartphone. In our experiments, this system showed sub-meter positioning accuracy.

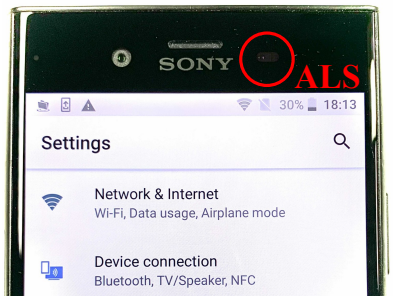

Fig. 1: An example of an ALS assembly in a smartphone.

The remainder of this paper is organized as follows. In Section II, we first introduce the ALS assembly in a smartphone and the constraints arising from its use by the smartphone OS. We then present a design for a VLP system using such an ALS in Section III. In Section IV, we describe our experimental evaluation of ALiSA. Related work is presented in Section VI. In Section V, we discuss the localization performance and limitations of our system. Section VII concludes the paper.

II. ALS

In this section, we first introduce the ALS assembly's sampling characteristics and then examine the constraints that the smartphone's OS imposes on the ALS.

A. ALS Primer

The ALS, as shown in Fig. 1, is a widely used light sensor in mobile devices that provides information about ambient light levels. A common application of ALS is the automatic dimming of the display under a variety of user environments, such as darkness or indoors, where multiple lights provide illumination, aiming to improve screen visibility and save battery power. One of the most significant advantages of the ALS assembly is its low power consumption (below 1 mW), which is much lower than that of cameras (about 2,000 mW) and high-speed PDs (about 150 mW) [8]. Therefore, ALS is suited to new applications in mobile devices because such devices are very sensitive to power consumption [9].

B. Frequency Response of the ALS

An ALS works as a frequency filter for transmitted signals. The features of the filter are explained by the integration effects related to the light-receiving characteristics of the ALS.

The ALS receives and converts the analogue transmitted signal to digital form using its internal light-receiving cells and outputs the integrated value of the signal received during a period T_s. If the fundamental frequency of the transmitted signal $s(t)$ is $1/(nT_s)$ (n: integer,$n \geqq 1$), the ALS's output $r(\delta)$ is

TABLE I: Examples of ALS sampling operations

Smartphone	Estimated sampling frequency[Hz]	Operation
Xperia XZ1	17.78	Uniform sampling with missing values
Galaxy S10+	less than 16.67	Nonuniform sampling
Google PIXEL4	9.78	Uniform sampling with missing values
ASUS ZenFone3	8.20	Uniform sampling with missing values

$$r(\delta) = \frac{1}{T_s}\int_0^{T_s} s(t+\delta n T_s)dt, \tag{1}$$

where δ is the clock delay ratio between the transmitted signal and the ALS. The Fourier coefficients of $s(t)$ and $r(\delta)$, denoted by S_k and R_k, respectively, are

$$S_k = \frac{1}{nT_s}\int_0^{nT_s} s(t)e^{-j2k\pi t/nT_s}dt, \tag{2}$$

and

$$R_k = \int_0^1 r(\delta)e^{-j2k\pi\delta}d\delta = S_k e^{jk\pi/n}\text{sinc}\,(k\pi/n). \tag{3}$$

When the transmitted signal of frequency $f_k = k/(nT_s) = (k/n)f_s$ is received by an ALS whose sampling frequency is denoted by $f_s = 1/T_s$, the received signal is the output of the frequency filter given by the following transfer function $H(k)$.

$$\begin{aligned} H(f_k) = \frac{R_k}{S_k} &= e^{jk\pi/n}\text{sinc}\,(k\pi/n) \\ &= e^{jf_k\pi/f_s}\text{sinc}\,(f_k\pi/f_s). \end{aligned} \tag{4}$$

where $\text{sinc}\ x = \frac{\sin x}{x}$.

Fig. 2 plots a theoretical model of the frequency response (Eq. (4)) and the normalized RSS when transmitted signals of different frequencies are received by the ALS assembly in a Sony Xperia XZ1. Fig. 2 shows that the RSS obtained by the ALS attenuates according to the theoretical model because of the integration effect. Moreover, when the frequency of the transmitted signal is above the Nyquist frequency [10], where it is affected by frequency aliasing, the RSS follows the original frequency response of the transmitted signal. For example, a signal of 200.519 Hz is aliased to 4.939 Hz and the RSS follows the frequency response of the 200.519-Hz signal. The details of the frequency aliasing are described in Section III-C. From our signal-reception experiments using the ALS assemblies in four different smartphones, we confirmed that the frequency response of ALS follows Eq. (4).

C. Constraints on the ALS Assembly in a Smartphone

1) Investigation of Sampling Operations: We have confirmed that the ALS assembly in a smartphone is restricted to a very low sampling frequency by the smartphone OS. The sampling operations cannot be controlled by user-level application software and the sampling frequency cannot be changed to an arbitrary value with arbitrary timing.

We conducted two additional experiments to investigate the sampling operations of these ALS assemblies. First, we

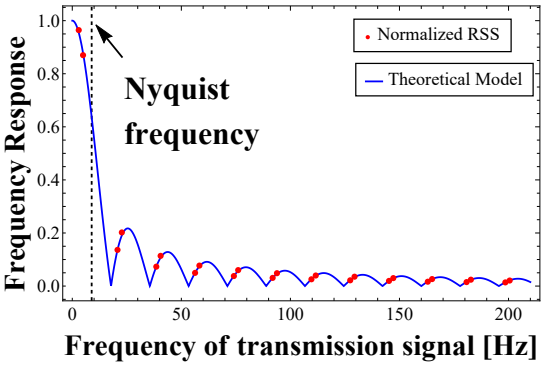

Fig. 2: RSS and the theoretical model of frequency response.

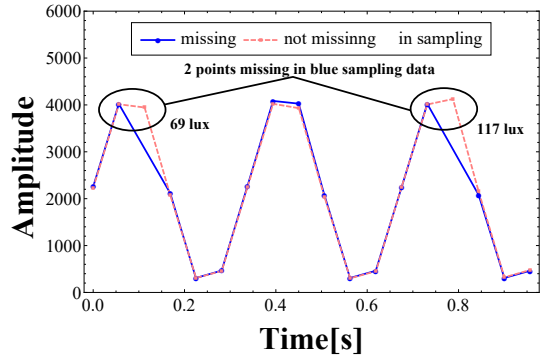

Fig. 3: Missing data in sample sets received by an ALS assembly in a smartphone

received multiple sinusoidal signals, whose frequencies were slightly different. Second, we made 1,000 measurements of sinusoidal signals modulated at 1 Hz. From our results, the sampling frequency of the ALS could be identified to within 0.01 Hz using the millisecond-order timestamp function provided by the Android Sensor application-programmer interface [11]. Table I shows the sampling operations for various ALS assemblies. According to this table, the sampling frequency of the ALS depends on the implementation within the smartphone. Some devices have sample sets with missing values, while only the Galaxy S10+ conducts nonuniform sampling.

Consider the Sony Xperia XZ1, whose ALS is an Avago APDS-9940-LIGHT that has a maximum sampling rate of about 300 Hz [12] [13]. However, when assembled in the smartphone, the sampling frequency is limited to 17.78 Hz, which seems to depend on a setting at the time of manufacture and cannot be changed by user application software such as Android Studio.

2) Sampling with Missing Values: We now describe the causes of missing values in the sample sets received by the

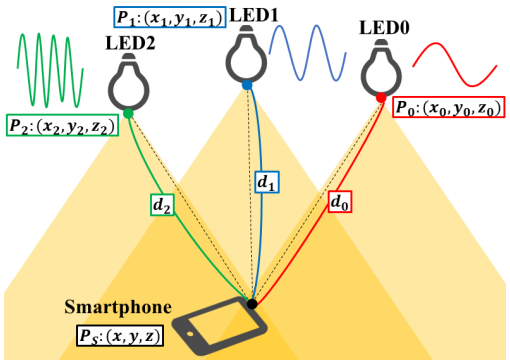

Fig. 4: An overview of ALiSA

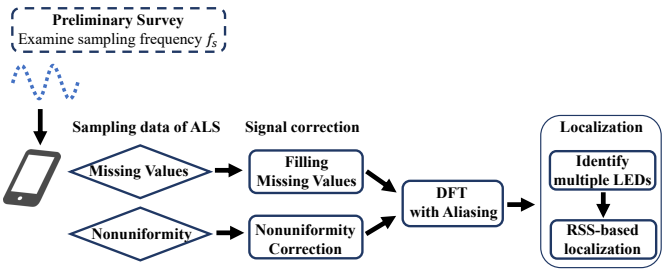

Fig. 5: Processing flow of the proposed method

ALS assemblies in smartphones. Fig. 3 shows two sample sets received by the ALS in a Sony Xperia XZ1, where the blue line has missing sample values and the red line has no missing values. In this figure, the sampling along the blue line involves two missing values within a 1-second interval. We consider that this is caused by the change between neighboring sampled RSS values being smaller than the light-intensity resolution of the ALS. That is, the ALS has not detected the change in the received signal, causing a missing-value issue to occur in the sampled data of the ALS.

Based on this investigation, any VLP system using the ALS assembly in a smartphone needs to be considered the following issues.

- It is impossible to control the sampling operation via a user application and the sampling frequency is limited to very low values.
- There are devices whose sampling operations lead to missing values.
- There are devices whose sampling is nonuniform.

III. Proposed Method

The proposed ALiSA system uses the illumination from multiple LEDs placed on a ceiling and a smartphone. Figs. 4 and 5 show an overview of the system and its processing flow, respectively. Each LED broadcasts a sinusoidal wave with its own individual frequency, which is received by the ALS assembly in a smartphone. We apply the proposed signal correction methods (filling missing values and nonuniformity correction) to rectify the sampling data captured by the ALS, and then decode the resulting signal using the DFT and frequency aliasing. To achieve localization, we first identify the various LEDs via their frequencies, and then calculate the coordinates of the smartphone by using the LED signals' RSS values and the known coordinates of the LED devices.

A. Filling Missing Values

We consider two methods for filling missing values methods, based on the investigations in Section II-C.2. In Section IV-B, we compare them experimentally in terms of frequency-analysis accuracy and adopt the better-performing method for the following positioning experiments described in Section IV-E.

1) Zeroth-order Interpolation Using the Value Before the Missing Value: As described in Section II-C.2, when the change in RSS between samples is less than the resolution of the ALS, the ALS cannot detect the change and there will be a missing value in the sample set. We can compensate by inserting the same sample value as that obtained in the previous sample.

2) Cubic Spline Interpolation: Alternatively, we can estimate the missing value by fitting the entire sample set, including the missing interval, to a smooth curve using cubic spline interpolation. Let r_i be the sampling value at time t_i according to the sampling rate. Missing values included in the N consecutive samples $(t_0, r_0), (t_1, r_1), ..., (t_{N-2}, r_{N-2}), (t_{N-1}, r_{N-1})$ $(0 \leq i \leq N-1)$ are approximated by third-order polynomials in each of the $N-1$ intervals.

B. Nonuniformity Correction

When the sampling of ALS assembly in a smartphone is nonuniform, we can convert N nonuniform samples (t_i, r_i) captured by the ALS into M uniform samples at sample rate T_s' by a least-squares method, according to the sampling theorem [10]. The degree b_{ij} by which the value p_j at the new sampling time $j \times T_s'$ is affected by the original data at time t_i is given as

$$b_{ij} = \mathrm{sinc}\frac{\pi(t_i - j \times T_s')}{T_s'}, \quad (0 \leq i \leq N-1, 0 \leq j \leq M-1). \tag{5}$$

The value $\boldsymbol{p} = (p_0, p_1, \cdots, p_{M-1})^T$ is then solvable by the following least-squares method using the influence matrix B of elements b_{ij} and the original sampling values $\boldsymbol{r} = (r_0, r_1, \cdots, r_{N-1})^T$ as follows.

$$\boldsymbol{p} = (B^T B)^{-1} B^T \boldsymbol{r}. \tag{6}$$

From the uniform data $\boldsymbol{p}$ obtained by Eq. (6), we can reproduce the original signal by following the sampling theorem, giving the $f(t)$ shown in Eq. (7).

$$f(t) = \sum_{j=0}^{M} p_j \mathrm{sinc}\frac{\pi(t - j \times T_s')}{T_s'}. \tag{7}$$

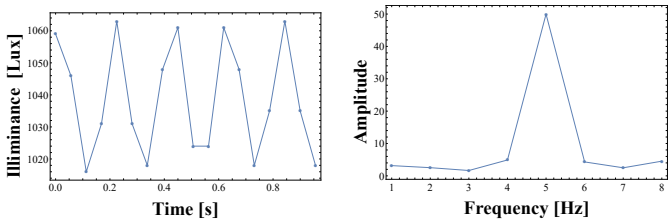

(a) time domain **(b)** frequency domain

Fig. 6: Examples of frequency aliasing: a 200.519-Hz transmitted signal is interpreted as a 4.939-Hz signal by the ALS, whose sampling frequency is 17.78 Hz.

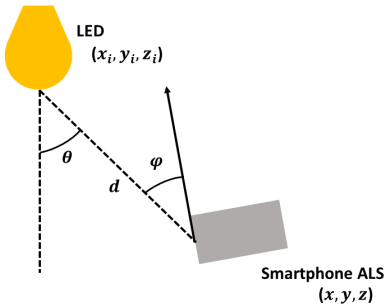

Fig. 7: A geometric model of localization algorithm

C. Frequency Aliasing

VLP systems convey the location information of LEDs through light signals modulated at F_{70}, which are perceived as flicker-free in human vision. However, the sampling frequency of the ALS assembly in a smartphone is 17.78 Hz at most (for the Sony Xperia XZ1, as shown in Table I) because of constraints applied by the smartphone OS. According to the sampling theorem, the ALS cannot correctly demodulate a light signal modulated at F_{70}. We therefore make use of frequency aliasing to decode the transmitted signals for LED identification.

When the modulated signal is sampled at a rate below the Nyquist frequency, the signal frequency calculated by the DFT is aliased in accordance with the following equation.

$$f_a = \min(f_o - (A-1)f_s, Af_s - f_o), \tag{8}$$

where f_a is the aliased frequency, f_o is the frequency of the transmitted signal, and f_s is the sampling frequency. A is the smallest natural number that satisfies $Af_s - f_o \geq 0$. Fig. 6 plots an example of frequency aliasing. By giving the aliased frequencies associated with individual LEDs to the system in advance, it is possible to identify the transmitted signals emitted from the various LEDs.

D. Localization Algorithm

After correcting the sampling data measured by the ALS and decoding the frequencies associated with multiple LEDs, we can calculate the smartphone position based on the principle of the trilateration. Each LED is identified by its modulation frequency, and the distance between the smartphone and the LED can be calculated by using the amplitude of its aliased signal from the DFT results. Fig. 7 shows a geometric model of our localization algorithm. In this model, by considering the frequency response $|H(f_k)|$ of the ALS, the RSS of the signal emitted from the LED follows Eq. 9, in accordance with a Lambertian radiation pattern [14].

$$P_r = C\sin(c\pi)|H(f_k)|\frac{\cos^l\theta\cos^m\varphi}{d^2}, \tag{9}$$

where P_r is the RSS obtained as spectrum magnitude values of the DFT and d is the distance between the LED and the ALS. C and $\sin(c\pi)$ are the maximum emission power and duty cycle of the LED, respectively. f_k is the frequency of the transmitted signal, $\cos^l\theta$ is the irradiation angle response of the LED, and $\cos^m\varphi$ is the incidence angle response of the ALS. l and m are called the "Lambertian orders", which depend on the individual LEDs and the ALS, respectively. We describe the measurement of l and m later (see Section IV-E.1).

In this paper, we assume that all LEDs are facing downward and that the smartphone is parallel to the floor. In this case, let the coordinates of the i-th LED and smartphone be (x_i, y_i, z_i) and (x, y, z), respectively, for which $\theta = \varphi$ and $\cos\theta = \cos\varphi = |z_i - z|/d_i$ hold. We can then calculate the distance d_i between the i-th LED and smartphone from Eq. (9).

Four or more distances d_i obtained by Eq. (9) can then be used to calculate the smartphone coordinates (x, y, z). If more than four LEDs are installed on the ceiling, then we treat this as an optimization problem, as follows.

$$\arg\min_{x,y,z}\sum_i(\sqrt{(x-x_i)^2+(y-y_i)^2+(z-z_i)^2}-d_i)^2. \tag{10}$$

In this paper, we use the Levenberg–Marquardt algorithm (LMA) [15] [16], an extension of the least-squares method, to solve Eq. (10) as an unconstrained nonlinear optimization problem.

IV. Experimental Evaluation

In this section, we first investigated the effectiveness of the proposed signal-correction methods, namely the two filling-missing-values methods and the nonuniformity correction method. We then evaluated the signal-reception performance of an ALS assembly in a smartphone. Finally, we evaluated the localization performance of ALiSA in various experimental settings.

A. Experimental Environment

The LED transmitter used was a BXRE-50C4001-B-74 model from Bridgelux [17] attached to a heat sink. All the LEDs used pulse density modulation (PDM), obtained by delta-sigma modulation [18], to generate sinusoidal signals. A 5-V pulse signal from a function generator (NF Corporation WF-1948) was amplified to 35 V using a power driver and power supply. The LEDs therefore flickered at the PDM rate (i.e., at high frequency), and the signal received by the

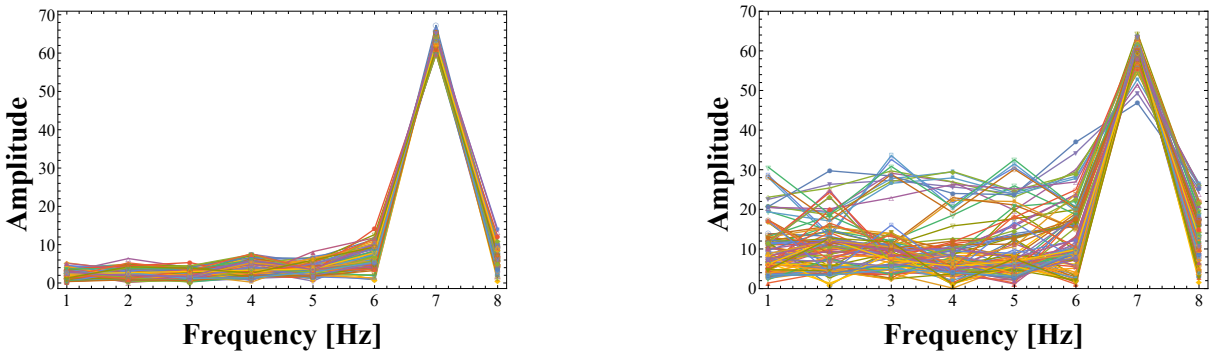

(a) Zeroth-order interpolation **(b)** Cubic spline interpolation

Fig. 8: Frequency spectra of interpolated signals (100 measurements)

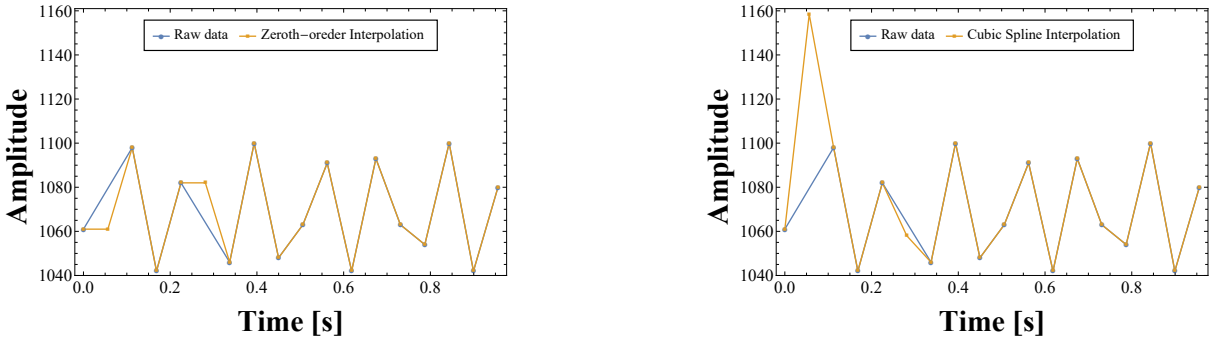

(a) Zeroth-order interpolation **(b)** Cubic spline interpolation

Fig. 9: Comparisons of the reproduced signals using different interpolation methods

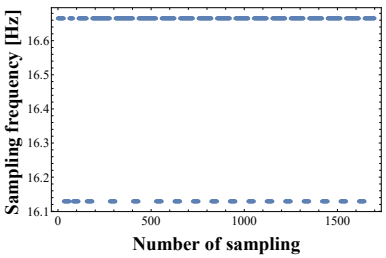

Fig. 10: Transition of Galaxy S10+ sampling frequency

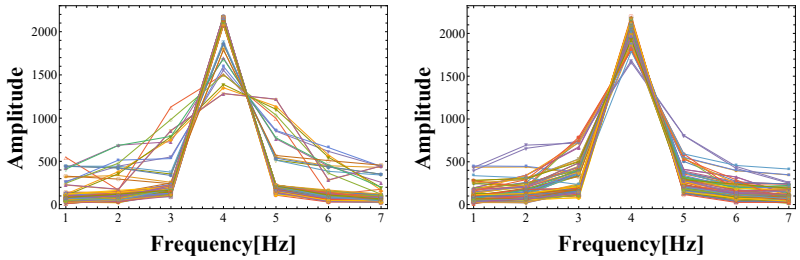

(a) Uncorrected **(b)** Corrected for nonuniformity

Fig. 11: Frequency spectra for uncorrected and corrected signals for 100 measurements)

ALS was recorded as a sinusoidal wave. As explained in Section III, ALiSA decodes the received signal via a DFT, utilizing frequency aliasing and identifying the LEDs in terms of their flicker frequency. We set each flicker frequency $f_{i,A}$ as follows.

$$f_{i,A} = (i/n + A)f_s = f_{i+An}, \tag{11}$$

where i is the LED ID, set to an integer value from 1 to $(n/2)$ to avoid incorrect identification caused by frequency aliasing. f_s is the sampling frequency of the ALS, n is the number of DFT samples, and f_s/n is the fundamental frequency of the transmitted signal. A was an integer chosen to make the LEDs appear flicker-free. In all experiments, we used the ALS assembly in a smartphone to record the received signal from the LEDs, with the smartphone being aligned horizontally on a tripod. The proposed method was then applied to these recorded data offline.

B. Evaluation of Methods for Filling Missing Values

We compared experimentally the two methods for filling missing values described in Section III-A to evaluate their relative effectiveness. We used the Avago APDS-9940 LIGHT assembly in a Sony Xperia XZ1 as the ALS receiver. Its sampling frequency was 17.78 Hz and there were missing values in the sample set, as shown in Table I. This ALS output illuminance values from 1 lx to 50000 lx, and the maximum power consumption was 0.11 mA. Following Eq. (11), we set the fundamental frequency of the transmitted signal $f_s/n = 17.78/18 \approx .0.988$.

Fig. 8 shows the frequency spectra for 100 measurements when the transmitted signal of 202.494 Hz received by the ALS was corrected by the two proposed methods for filling

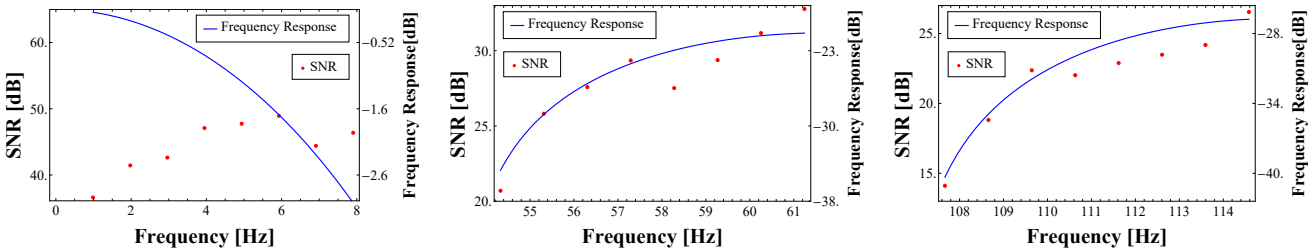

(a) Band 1: 0.988 Hz to 7.902 Hz **(b)** Band 2: 54.328 Hz to 51.242 Hz **(c)** Band 3: 107.668 H to 114.582 Hz

Fig. 12**:** Average SNR and frequency response of transmitted signals (the blue lines are derived from Eq. 4

.

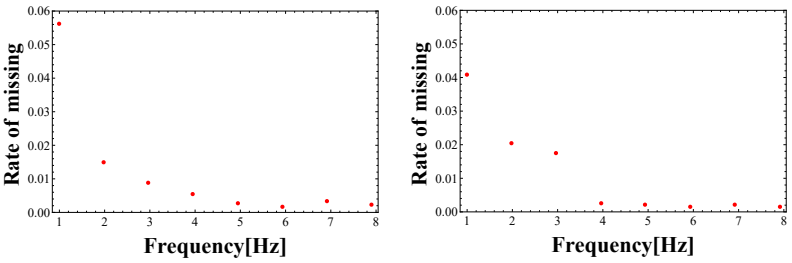

(a) Real sampling by ALS **(b)** Simulation

Fig. 13**:** Average rates of missing sampling values for Band 1: 0.988 Hz to 7.902 Hz

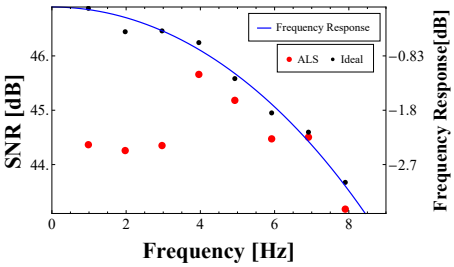

Fig. 14**:** Average SNR and frequency response for the simulation, where black points show ideal sampling and red points show missing-value sampling

missing values. We found that both methods correctly decoded the transmitted signal as a signal of aliased frequency 6.914 Hz $(= 202.494 - 11 \times 17.78)$. However, we noticed that the sidelobes on the spectrum of cubic spline interpolation were greater than that of zeroth-order interpolation. We consider that this was because, when the initial sampled data are missing, the interpolation values in cubic spline interpolation can diverge, and the quantization error therefore increases (see Fig. 9). This meant that the zeroth-order interpolation method could reproduce missing values in the sampled data more accurately. We therefore used this method in the later evaluation experiments described in this paper.

C. Evaluation of Methods for Nonuniformity Correction

In this experiment, we used the AMS TCS3407 assembly in a Galaxy S10+ as the ALS receiver, because only Galaxy S10+ had nonuniform sampling among the tested smartphone, as shown in Table I. Its sampling frequency was less than 16.67 Hz.

Fig. 10 shows the transition of sampling frequencies. The frequency spectra for uncorrected data and data corrected for nonuniformity (100 consecutive sampling measurements) are shown in Fig. 11. We found that the proposed method for nonuniformity correction reduced the magnitude of the sidelobes.

D. Experiments on ALS Signal Reception

We evaluated the signal reception performance of an ALS assembly in a smartphone. This was an important experiment because the reception performance greatly affects the localization results. We measured the SNR of the signal received by an ALS responding to the emission from a single LED. However, the ALS assembly in a smartphone cannot receive a direct-current (0 Hz) signal because of the missing-value behavior described in Section II-C.2. This means that it cannot measure the noise power on its own. We therefore used the average power from the DFT output, excluding the power of the target frequency, as the noise power. We used the Avago APDS-9940 LIGHT assembly in a Sony Xperia XZ1 as the ALS receiver, and applied zeroth-order interpolation to correct for missing values in the received signal. For all these experiments, the number of DFT samples n was set to 18. We considered three frequency bands, the fundamental frequency (order $k = 1$) of which was $f_s/n = 17.78/18 \approx .0.988$ Hz. The three transmitted-signal frequency bands were as follows.

Band 1: 0.988 Hz – 7.902 Hz ($k = 1$ – 8),

Band 2: 54.328 Hz – 61.242 Hz ($k = 55$ – 62),

Band 3: 107.668 Hz – 114.582 Hz ($k = 109$ – 116).

1) Frequency of Transmitted Signals: We first evaluated the SNR for the three different frequencies of transmitted signals. Fig. 12 shows the average SNR and frequency response of the transmitted signals for each frequency band. The value of frequency response, theoretically derived from Equation (4) in Section II-B, corresponds to the magnitude ratio between the transmitted and received signals (without noises), and depends on the frequencies of the transmitted signal (f_k) and the ALS sampling (f_s). From the blue lines in Fig. 12, we confirmed that the higher the frequency of the transmitted signal, the smaller the frequency response. The red points in the figure represent SNRs calculated using received signals by the ALS in real environments (with noises). From Fig. 12, we found that the SNR decreased with the attenuation of the frequency response, as given in Eq. (4).

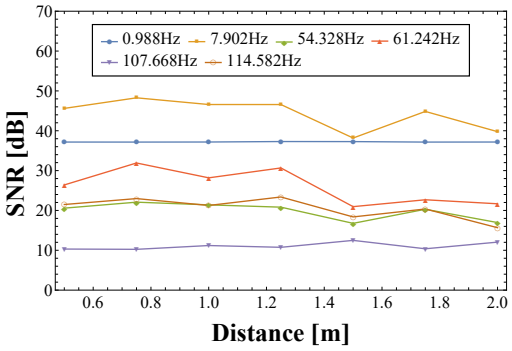

Fig. 15: The average SNR at different measurement distances and frequencies

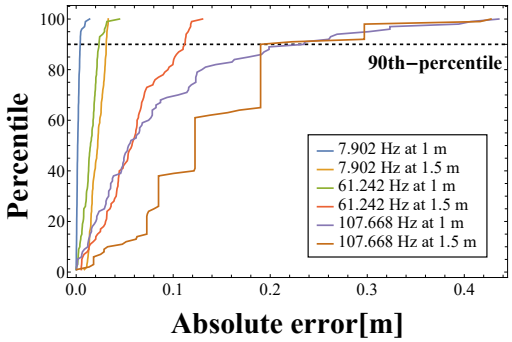

Fig. 16: Cumulative error functions for distance measurements at different distances and frequencies

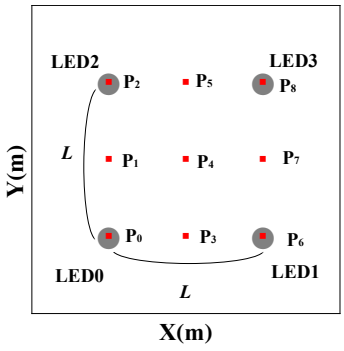

Fig. 17: Arrangement of LEDs and measurement points

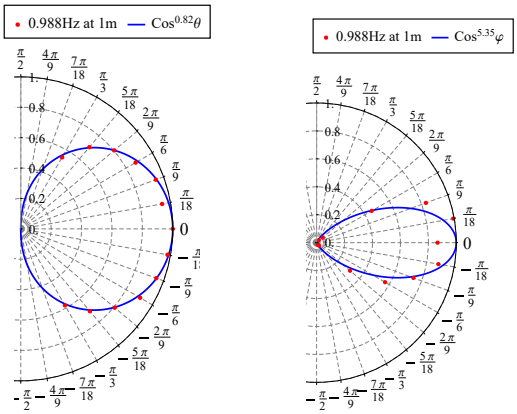

(a) Irradiation angle response to the LEDs

(b) Incidence angle response of the ALS

Fig. 18: Angle responses based on the normalized received-signal power

However, the SNR for frequencies below 4.939 Hz decreased significantly, as shown in Fig. 12a. This is related to the missing values in the received signal (see Fig. 13a), where we found that the lower the frequency, the higher the missing-sample rate for the received signal in this frequency band. Furthermore, the noise introduced by the method for filling missing values is not Gaussian, preventing its attenuation via signal averaging over 100 measurements. This means that the accurate estimation of target frequencies is difficult.

To examine the effect of missing-value sampling on the SNR, we conducted SNR measurement experiments, comparing a simulation of the ideal sampling condition (no missing values) to an actual ALS sampling condition (with missing values). Its average missing rate is shown in Fig. 13b. In Fig. 14, discrete points represent the average SNRs for the simulation, where the black points are the SNRs for ideal sampling and the red points are the SNRs for ALS sampling. There were 100 measurements at each frequency. The blue line representing frequency responses is given by Eq. (4). Based on these results, we can confirm that the SNRs obtained by ALS and ideal sampling fit well to the blue line but those by ALS sampling decrease because of missing values.

2) Working Distances: Next, we changed the linear distance between the LED and the ALS from 0.5 m to 2.0 m and again measured the SNRs. Fig. 15 shows the average SNR at each distance for each frequency, and Fig. 16 shows the cumulative error function for distance measurements at 1.0 m and 1.5 m for 7.902 Hz (highest SNR), 61.242 Hz (middle SNR), and 107.668 Hz (lowest SNR). The results shown in Fig. 15 confirm that the SNRs obtained at different distances follow the experimental and theoretical results shown in Fig 12. However, Fig. 15 also shows that the distance does not significantly affect the SNR. Investigations regarding this issue are needed in our future work.

Fig. 16 indicates that signals with better SNRs tend to give a smaller error in distance measurements. Moreover, the greater the distance between the LED and ALS, the worse the standard deviation of the distance measurement error, because the standard deviation of the SNR increases as the RSS is attenuated, in accordance with Eq. (9). However, the signal at 107.668 Hz (lowest SNR) did not follow Eq. (9) as both the distance and the error in distance measurement increased. This seems to be because the change in the light signal is small, leading to 80% of its sample data representing missing values. However, the target frequency in the DFT results could still be identified by applying our proposed method for filling missing values.

E. Experiments on Localization Performance

To evaluate the localization performance of our VLP system using the ALS assembly in a smartphone, we conducted several experiments that used four LEDs installed on the ceiling of our laboratory in a square array, as shown in Fig.

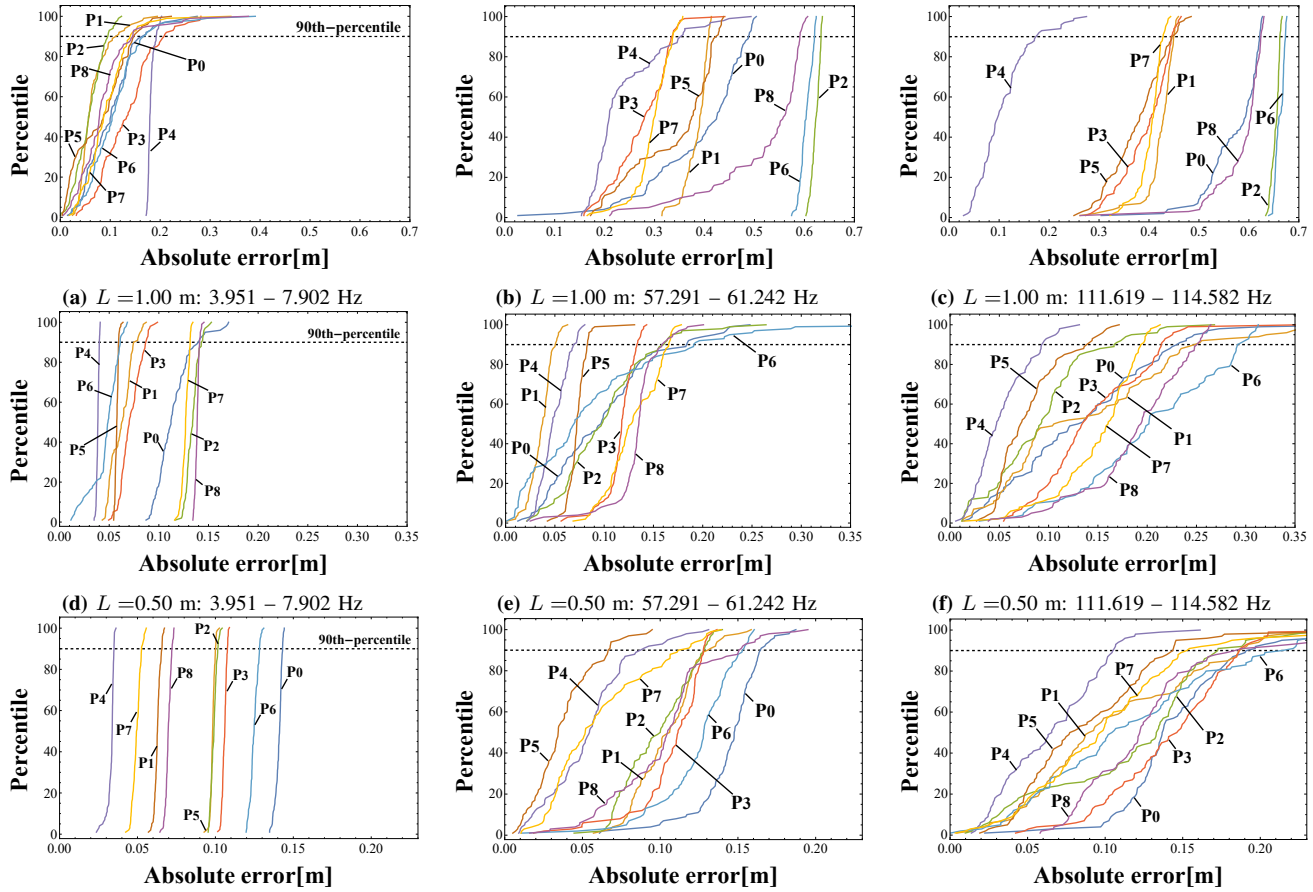

Fig. 19: Cumulative distribution function of positioning errors for each LED separation distance L and signal frequency band

TABLE II: Frequency patterns for transmitted signals

	LED0[Hz]	LED1[Hz]	LED2[Hz]	LED3[Hz]
Band 1	3.951	4.939	5.927	7.902
Band 2	57.291	59.267	60.254	61.242
Band 3	111.619	112.607	113.594	114.582

17. The height of the ceiling was 2.22 m. We placed LED0 at (1.00 m, 1.00 m, and 2.22 m), and experimented with three LED separation distances L = 1.0 m, 0.50 m, and 0.25 m.

Each of the four LEDs was assigned to one of the three frequency patterns (see Table II), which showed the better of the SNR results (see Fig. 12). The localization experiments therefore involved 9 different settings (3 distances × 3 frequency patterns). We used the Avago APDS-9940 LIGHT assembly in a Sony Xperia XZ1 as the ALS receiver, and placed it horizontally at a height of 1.40 m above the floor, below each of the nine points shown in Fig. 17. These ground truth points were measured by using a COTS laser range sensor (LEICA DIST S510) and a semicircular protractor to obtain their distances and angles, respectively. The ALS receiver received the signals from the four LEDs and its 2-D coordinates were calculated offline. The measurement at each point was repeated 100 times. The number of samples n was set to 18.

1) Irradiation and Incidence Angle Responses: To calculate the smartphone coordinates using Eq. (9), we first obtained the Lambertian orders l and m for the irradiation angle response to the LEDs and the incidence angle response of the ALS, respectively. We placed the smartphone one meter away from LED and changed the angles θ and phi in Eq. (9) from $-\frac{\pi}{3}$ to $\frac{\pi}{3}$ at $\frac{\pi}{18}$ intervals as shown in Fig. 18. 300 measurements were conducted at each angle. By using the obtained measurement values at different angles, we applied the least squared method to make the absolute error of Eq. (9) minimum. From these results, we obtained the Lambertian order values $l = 0.82$ and $m = 5.35$, respectively.

2) 2-D Localization Results: Fig. 19 shows the cumulative distribution function for the 2-D localization errors for each LED separation distance L and for each signal frequency pattern. The maximum 90th-percentile errors for the estimated position of the smartphone for each separation distance L are shown in Table III, respectively.

V. Discussion

A. Localization Evaluation

We evaluated the localization results with respect to systematic and random errors. We denote $\boldsymbol{x}_i^p$ $(i = 1, 2, ..., N)$ as the i-th positioning result for any measurement position p, $\bar{\boldsymbol{x}}^p = (1/N)\sum_i \boldsymbol{x}_i^p$ as its mean, and $\boldsymbol{X}^p$ as the true position. The errors were calculated using the following formulae:

TABLE III: The Maximum 90th-percentile errors for the estimated position of the smartphone

L [m]	Maximum 90th-percentile error [m]		
	Band 1	Band 2	Band 3
1.0	0.21	0.63	0.67
0.50	0.14	0.19	0.29
0.25	0.14	0.16	0.21

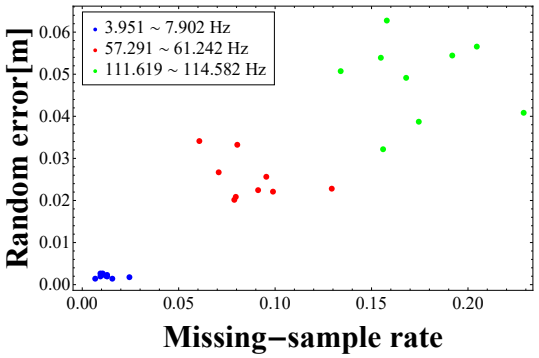

Fig. 20: Average missing-sample rate vs. random positioning errors

- Systematic error: $|\boldsymbol{X}^p - \bar{\boldsymbol{x}}^p|$,
- Random error: $\sqrt{(1/N)\sum_i |\boldsymbol{x}_i^p - \bar{\boldsymbol{x}}^p|^2}$.

1) Systematic Errors: Figs. 19a – 19c show that the average systematic errors at $L = 1.0$ m were 0.07 m, 0.40 m, and 0.46 m, respectively. Figs. 19d – 19f show that the average systematic errors at $L = 0.5$ m were 0.09 m, 0.09 m, and 0.11 m respectively. Figs. 19g – 19i show that the average systematic errors at $L = 0.25$ m were 0.09 m, 0.08 m, and 0.09 m, respectively. One cause of the systematic errors seems related to inaccurate placement of the experimental equipment and smartphone during the experiments. In addition, as shown in Figs.19b and 19c, RSS values obtained by the ALS at particular measurement points (P2 and P6) deviated from the Lambertian radiation pattern because the SNR decreased under the influence of the frequency response.

2) Random Errors: We can evaluate random errors in terms of the missing-sample rate in the received signals. Fig. 20 shows the average missing-sample rate and random errors at the nine measurement points when L was set to 0.25 m (see Figs. 19g – 19i). The means, standard deviations and maximum values of the random errors calculated using all the data at all the measurement points were 0.0021 m, 0.0004 m and 0.0026 m using Band 1, 0.0253 m, 0.0052 m and 0.0341 m using Band 2, and 0.0488 m, 0.0098 m and 0.0628 m using the Band3 signals, respectively.

As the frequency of the transmitted signal increases, the missing-sample rate and random positioning error increase. This is because the SNR decreases as the frequency increases under the influence of the frequency response and the increase in the number of missing values.

3) 3-D Localization: Section IV-E.2 describes our 2-D localization experiments, for which the height of the smartphone was known. In principle, the proposed VLP system can conduct 3-D localization of a smartphone when its height is unknown. The 3-D localization results for a LED separation distance of $L = 0.25$ m are shown in Fig. 21. These results indicate that the LMA used in the proposed method cannot calculate a global optimal solution because of the complexity of the objective function in Eqs. (9) and (10). A nonlinear optimization method could be considered for obtaining a global optimum solution, as described in [19], to improve the 3-D localization accuracy.

4) Field of View (FoV): Fig. 18b indicates that the incident angle response of the ALS used in our experiments did not always follow the Lambertian radiation pattern, particularly between 0° and 20°. This is because the incorporation of the ALS into the smartphone, which involves the bezel shape, can affect its FoV. This is different from when other light sensors are used. We confirmed by experiment that the incident angle response of the ALS differs depending on the smartphone model used. Therefore, we consider that the directionality of the smartphone, the positional relationship between the LEDs and the smartphone, and the differences between smartphone models can all affect the positioning accuracy. Further investigation is needed into the incident angle response of the ALS assembly in a smartphone.

B. Number of Frequencies as Location IDs

In our system, we decode the received signal using the DFT with frequency aliasing and identify the multiple LEDs via their different modulation frequencies. However, in an indoor environment where many LEDs are installed, it may be difficult to assign different frequencies to each LED because the sampling frequency of the ALS is very low, limiting the number of discrete frequencies available. It might therefore be necessary to devise an alternative frequency allocation method. Otherwise, if the localization space is limited to a single room or floor, for example, we can deploy the current version of the proposed VLP system. We plan to investigate the frequency allocation problem in future work.

C. Limitations and Challenges of the VLP System Using ALS

Assuming localization in a general indoor environment, the LEDs need to be modulated at F_{70} to make it difficult for human viewers to perceive light flicker. The experiments described in Section IV-E.2 indicate that high-precision localization using a low frequency signal is possible, and that localization using a signal modulated at F_{70} should be possible in principle. In addition, we have confirmed that the arrangement of LEDs in a square (of side 1 m or 0.5 m) was almost the same as or better than that used in a previous study [20]. Taking advantage of the low power consumption of an ALS and the acceptable level of positioning accuracy, the proposed method should be effective in enabling VLP systems to be used for applications such as gesture recognition within a limited positioning space, tracking systems that require longer-term operation, and navigation systems that require sub-meter-level positioning accuracy. However, the localization using a signal modulated at F_{70} has a low accuracy. To fix this problem, we could consider improving the SNR by increasing the transmitted signal power. Another possibility for improving

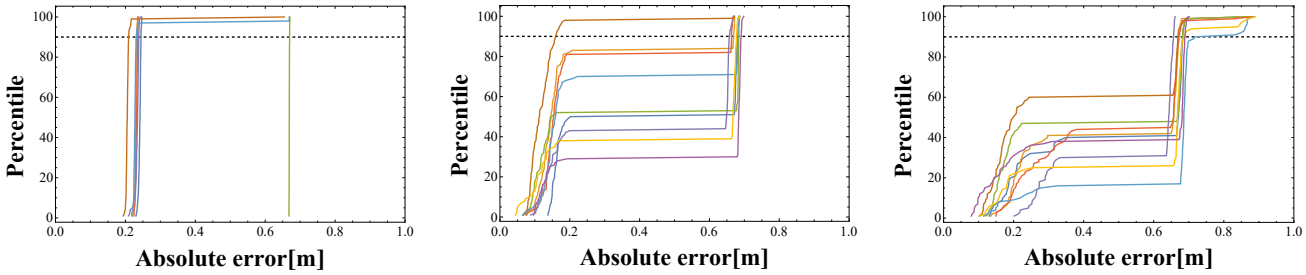

(a) L =0.25 m: 3.951 – 7.902 Hz **(b)** L =0.25 m: 57.291 – 61.242 Hz **(c)** L =0.25 m: 111.619 – 114.582 Hz

Fig. 21: Cumulative distribution function for 3-D positioning errors

the VLP system performance is to use the camera and ALS assembly in the smartphone alternately, retaining the positioning performance while managing the energy consumption.

VI. Related Work

A. VLP

Most VLP systems utilize a CMOS camera or a light sensor as a receiver [7] [21]. Camera-based systems [22] [23] [24] achieve sub-meter-level positioning accuracy based on the "rolling shatter effect" [25] [26]. However, high power consumption is required for camera-based systems. Proposed approaches using light sensors include time of arrival [27], time difference of arrival [28], angle of arrival (AoA) [29], and RSS-based methods [30]. Because these systems are expected to use high-speed PDs, they would require additional equipment in the smartphone.

B. Applications Using ALS

The ALS is a receiver suitable for long-term operation of VLP systems in smartphones because it is widely installed in modern smartphones and involves lower power consumption than that for a camera or high-speed PD. To date, a small number of VLP systems using an ALS have been proposed. ALS-P [20] identifies LEDs by using aliasing frequencies calculated from two sampling frequencies for the ALS. The results of RSS-based positioning give 90th-percentile errors of less than 0.25 m in a 1.5 m $\times$ 1.2 m environment with four LEDs. NALoc [8] utilizes the nonlinear characteristics of ALS to detect the beat signal from transmitted signals modulated at two different frequencies, from which it can identify multiple LEDs. Pulsar [31] utilizes dual ALSs to realize highly accurate AoA-based localization. However, these systems do not utilize the ALS assembly in a smartphone. They control an ALS installed on a microcomputer board (Arduino in [20], the exact model name not written in [8]), and their sampling frequency is set to more than 100 Hz. In the investigations described in this paper, we found that it is difficult to control the sampling operations of the ALS via user-level applications running on real smartphones and that the sampling frequency is at most 17.78 Hz. Therefore, with these realistic constraints, these previous proposals could not be implemented on a smartphone.

Some gesture recognition systems [32] [33] [34] and intelligent lighting systems [35] using the ALS assembly in a smartphone have been proposed. However, to the best of our knowledge, ALiSA is the first VLP system using the ALS assembly in a smartphone as a single receiver.

VII. Conclusions and Future Work

In the work described in this paper, we have investigated the sampling operation of the ALS assembly in a smartphone and developed a VLP system called ALiSA. We propose signal correction methods for the missing and nonuniform sampling data received by the ALS, which enables identification of the illuminating LEDs via DFT processing and their aliased frequencies. Our experimental results show that transmitted signals from multiple-LED illumination modulated at frequencies above 70 Hz can be correctly identified, and a 90th-percentile 2D positioning error with low frequency signals is less than 0.21 m for a room illuminated by four LEDs arranged in a 1-m square on the ceiling at 2.22 meters height, where the smartphone is placed parallel on the floor from 1.4 meters height. Those using high frequency signals in the same room setting show a 50th-percentile 2D position error of less than 0.44 meter. The position calculation is offline and not implemented on real time.

In future work, we will extend ALiSA and develop plans for applications that can be deployed in realistic situations.

Acknowledgement

This work was supported by JSPS KAKENHI Grant Number 19H04222 and 20K21781.

References

[1] Research and Markets. Indoor positioning and indoor navigation (IPIN) - global market trajectory & analytics. https://www.researchandmarkets.com/reports/5030011/indoor-positioning-and-indoor-navigation-ipin. (Accessed on 10/24/2020).

[2] F. Zafari, A. Gkelias, and K. K. Leung. A survey of indoor localization systems and technologies. *IEEE Communications Surveys Tutorials*, 21(3):2568–2599, 2019.

[3] T. Komine and M. Nakagawa. Fundamental analysis for visible-light communication system using LED lights. *IEEE Transactions on Consumer Electronics*, 50(1):100–107, 2004.

[4] P. H. Pathak, X. Feng, P. Hu, and P. Mohapatra. Visible light communication, networking, and sensing: A survey, potential and challenges. *IEEE Communications Surveys Tutorials*, 17(4):2047–2077, 2015.

[5] J. Armstrong, Y. A. Sekercioglu, and A. Neild. Visible light positioning: a roadmap for international standardization. *IEEE Communications Magazine*, 51(12):68–73, 2013.

[6] A. Wilkins, J. Veitch, and B. Lehman. LED lighting flicker and potential health concerns: IEEE standard PAR1789 update. In *2010 IEEE Energy Conversion Congress and Exposition*, pages 171–178, 2010.

[7] M. Afzalan and F. Jazizadeh. Indoor positioning based on visible light communication: A performance-based survey of real-world prototypes. *ACM Comput. Surv.*, 52(2), May 2019.

[8] L. Yang, Z. Wang, W. Wang, and Q. Zhang. NALoc: Nonlinear ambient-light-sensor-based localization system. *Proc. ACM Interact. Mob. Wearable Ubiquitous Technol.*, 2(4), December 2018.

[9] ROHM Semiconductor. Ambient light sensor (ALS) applicaions in portable electronics, 2013.

[10] A. J. Jerri. The Shannon sampling theorem-its various extensions and applications: A tutorial review. *Proceedings of the IEEE*, 65(11):1565–1596, 1977.

[11] Sensors overview — android developers. https://developer.android.com/guide/topics/sensors/sensors_overview. (Accessed on 12/17/2020).

[12] BROADCOM. APDS-9930. https://www.broadcom.com/products/optical-sensors/integrated-ambient-light-proximity-sensors/apds-9930. (Accessed on 12/28/2020).

[13] BROADCOM. APDS-9950. https://www.broadcom.com/products/optical-sensors/integrated-ambient-light-proximity-sensors/apds-9950. (Accessed on 12/28/2020).

[14] J. Grubor, S. Randel, K. Langer, and J. W. Walewski. Broadband information broadcasting using LED-based interior lighting. *Journal of Lightwave Technology*, 26(24):3883–3892, 2008.

[15] K. Levenberg. A method for the solution of certain non-linear problems in least squares. *Quarterly of Applied Mathematics*, 2(2):164–168, 1944.

[16] D. W. Marquardt. An algorithm for least-squares estimation of non-linear parameters. *Journal of the Society for Industrial and Applied Mathematics*, 11(2):431–441, 1963.

[17] Bridgelux LED Lighting V Series V18B-Gen8 / V18C-Gen 8. https://www.bridgelux.com/products/v-series#specifications. (Accessed on 01/27/2021).

[18] R. Schreier, S. Pavan, and G.C. Temes. *Understanding Delta-Sigma Data Converters*. IEEE Press Series on Microelectronic Systems. Wiley, 2017.

[19] B. Zhou, A. Liu, and V. Lau. Visible light-based user position, orientation and channel estimation using self-adaptive location-domain grid sampling. *IEEE Transactions on Wireless Communications*, 19(7):5025–5039, 2020.

[20] Z. Wang, Z. Yang, Q. Huang, L. Yang, and Q. Zhang. ALS-P: Light weight visible light positioning via ambient light sensor. In *IEEE INFOCOM 2019 - IEEE Conference on Computer Communications*, pages 1306–1314, 2019.

[21] Y. Zhuang, L. Hua, L. Qi, J. Yang, P. Cao, Y. Cao, Y. Wu, J. Thompson, and H. Haas. A survey of positioning systems using visible LED lights. *IEEE Communications Surveys Tutorials*, 20(3):1963–1988, 2018.

[22] S. Shimada, H. Hashizume, and M. Sugimoto. RefRec: Indoor positioning using a camera recording floor reflections of lights. In *Proceedings of UBICOMM 2022*, pages 57–63, 2020.

[23] Y. S. Kuo, P. Pannuto, K. J. Hsiao, and P. Dutta. Luxapose: Indoor positioning with mobile phones and visible light. In *Proceedings of the 20th Annual International Conference on Mobile Computing and Networking*, MobiCom '14, pages 447–458, New York, NY, USA, 2014. Association for Computing Machinery.

[24] C. Zhang and X. Zhang. LiTell: Robust indoor localization using unmodified light fixtures. In *Proceedings of the 22nd Annual International Conference on Mobile Computing and Networking*, MobiCom '16, pages 230–242, New York, NY, USA, 2016. Association for Computing Machinery.

[25] C. Liang, L. Chang, and H. H. Chen. Analysis and compensation of rolling shutter effect. *IEEE Transactions on Image Processing*, 17(8):1323–1330, 2008.

[26] H. Y. Lee, H. M. Lin, Y. L. Wei, H. I. Wu, H. M. Tsai, and K. C. J. Lin. RollingLight: Enabling line-of-sight light-to-camera communications. In *Proceedings of the 13th Annual International Conference on Mobile Systems, Applications, and Services*, MobiSys '15, pages 167–180, New York, NY, USA, 2015. Association for Computing Machinery.

[27] T. Q. Wang, Y. A. Sekercioglu, A. Neild, and J. Armstrong. Position accuracy of time-of-arrival based ranging using visible light with application in indoor localization systems. *Journal of Lightwave Technology*, 31(20):3302–3308, 2013.

[28] S. Jung, S. Hann, and C. Park. TDOA-based optical wireless indoor localization using LED ceiling lamps. *IEEE Transactions on Consumer Electronics*, 57(4):1592–1597, 2011.

[29] S. Yang, H. Kim, Y. Son, and S. Han. Three-dimensional visible light indoor localization using AOA and RSS with multiple optical receivers. *Journal of Lightwave Technology*, 32(14):2480–2485, 2014.

[30] L. Li, P. Hu, C.Peng, G. Shen, and F. Zhao. Epsilon: A visible light based positioning system. In *Proceedings of the 11th USENIX Conference on Networked Systems Design and Implementation*, NSDI'14, pages 331–343, USA, 2014. USENIX Association.

[31] C. Zhang and X. Zhang. Pulsar: Towards ubiquitous visible light localization. In *Proceedings of the 23rd Annual International Conference on Mobile Computing and Networking*, MobiCom '17, pages 208–221, New York, NY, USA, 2017. Association for Computing Machinery.

[32] M. A. Alawami, W. Aiken, and H. Kim. LightLock: User identification system using light intensity readings on smartphones. *IEEE Sensors Journal*, 20(5):2710–2721, 2020.

[33] E. Wen, W. Seah, B. Ng, X. Liu, and J. Cao. UbiTouch: Ubiquitous smartphone touchpads using built-in proximity and ambient light sensors. In *Proceedings of the 2016 ACM International Joint Conference on Pervasive and Ubiquitous Computing*, UbiComp '16, pages 286–297, New York, NY, USA, 2016. Association for Computing Machinery.

[34] A. Holmes, S. Desai, and A. Nahapetian. LuxLeak: Capturing computing activity using smart device ambient light sensors. In *Proceedings of the 2nd Workshop on Experiences in the Design and Implementation of Smart Objects*, SmartObjects '16, pages 47–52, New York, NY, USA, 2016. Association for Computing Machinery.

[35] T. K. Hariadi, A. K. H. Juwito, and A. N. N. Chamim. Smartphone-based lux meter with decision support system. In *2017 7th IEEE International Conference on Control System, Computing and Engineering (ICCSCE)*, pages 216–219, 2017.

Takuto Sato received the B.E. degree from Yamagata University, Yonezawa, Japan, in 2019. He is working for a Master's degree in information and science and technology from Hokkaido University, Sapporo Japan, advised by Prof. Masanori Sugimoto. His research interests include visible light positioning and mobile computing. He is a Student Member of the IPSJ.

Shota Shimada received the B.E. degree, and M.S. degree in information science and technology from Hokkaido University, Sapporo, Japan, in 2016, 2018, respectively. He is currently pursuing the Ph.D. degree in information science and technology with Hokkaido University. His research interests include visible light communication and visible light positioning.

Hiroaki Murakami received the B.E. degree, M.S. and Ph.D. degrees in information science and technology from Hokkaido University, Sapporo, Japan, in 2016, 2018, and 2021 respectively. He is currently a Project Researcher with the Graduate School of Engineering, The University of Tokyo, Tokyo, Japan. His research interests include ubiquitous and mobile computing. He is a member of the IPSJ.

Hiroki Watanabe received the B.E. and M.E., and D.E. degree from Kobe University in 2012, 2014, and 2017, respectively. He is currently an assistant professor with the Graduate School of Information Science and Technology, Hokkaido University, Sapporo, Japan. He is working on wearable computing and ubiquitous computing.

Hiromichi Hashizume (M ' 05) received the B.E., M.E., and D.E. degrees in electronic engineering from the University of Tokyo, Tokyo, Japan, in 1979, 1981, and 1984, respectively. He is currently a Professor with the Information Systems Architecture Science Research Division, National Institute of Informatics, Japan. His research field was computer networks and telecommunication, however, recently his interest has shifted to mathematical modeling of communication systems.

Masanori Sugimoto (M ' 97) received the B.E., M.E., and D.E. degrees in aeronautics and astronautics from the University of Tokyo, Tokyo, Japan, in 1990, 1992 and 1995, respectively. He is currently a Professor with the Graduate School of Information Science and Technology, Hokkaido University, Sapporo, Japan. His research interests include acoustic engineering, signal processing, artificial intelligence, and human-computer interaction technologies for designing smart systems and environments.